ACS OMEGA

http://pubs.acs.org/journal/acsodf

Article

Cell Protection and Crystal Endocytosis Inhibition by Sulfated *Laminaria* Polysaccharides Against Nano-COM-Induced Oxidative Damage in Renal Epithelial Cells

Bang-Xian Yu,[§] Yi-Han Zhang,[§] Chun-Yao Li,[§] Jun-Yi Xian,[§] Shu-Jue Li, Wei-Bo Huang, Ling-Hong Huang, and Xin-Yuan Sun*

Cite This: *ACS Omega* 2023, 8, 7816−7828

Read Online

ACCESS | Metrics & More | Article Recommendations

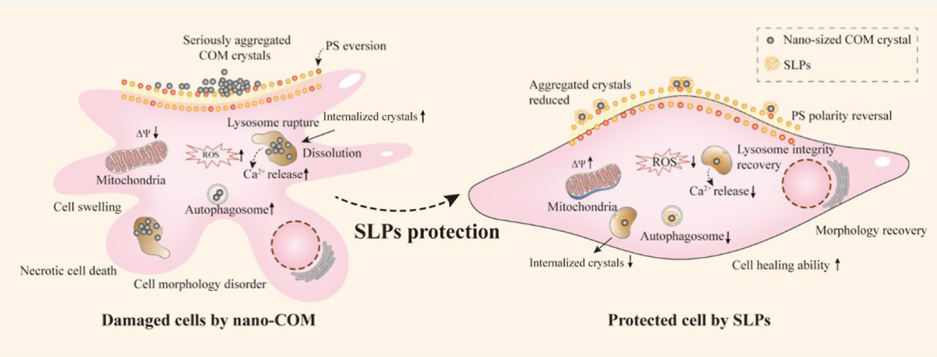

ABSTRACT: **Background**: The damage to renal tubular epithelial cells is closely related to the formation of kidney stones. At present, research on drugs that can protect cells from damage remains limited. **Methods**: This study aims to explore the protective effects of four different sulfate groups ($-OSO_3^-$) of *Laminaria* polysaccharides (SLPs) on human kidney proximal tubular epithelial (HK-2) cells and determine the difference in the endocytosis of nano-sized calcium oxalate monohydrate (COM) crystals before and after protection. COM with a size of 230 ± 80 nm was used to damage HK-2 cells to establish a damage model. The protection capability of SLPs (LP0, SLP1, SLP2, and SLP3) with $-OSO_3^-$ contents of 0.73, 15, 23, and 31%, respectively, against COM crystal damage and the effect of SLPs on the endocytosis of COM crystals were studied. **Results**: Compared with that of the SLP-unprotected COM-injured group, the cell viability of the SLP-protected group was improved, healing capability was enhanced, cell morphology was restored, production of reactive oxygen species was reduced, mitochondrial membrane potential and lysosome integrity were increased, intracellular Ca^{2+} level and autophagy were decreased, cell mortality was reduced, and internalized COM crystals were lessened. The capability of SLPs to protect cells from damage and inhibit the endocytosis of crystals in cells enhanced with an increase in the $-OSO_3^-$ content of SLPs. **Conclusions**: SLPs with a high $-OSO_3^-$ content may become a potential green drug for preventing the formation of kidney stones.

1. INTRODUCTION

Kidney stone disease is a common and frequently occurring health problem worldwide, and its incidence is increasing annually. It easily recurs after surgery; the recurrence rate is approximately 50% in 5 years and can reach as high as 75% in 20 years.[1] The formation of kidney stones is a complex multistep process that involves urine supersaturation; crystal nucleation, growth, and aggregation; and crystal attachment to the cell surface.[2] Calcium oxalate monohydrate (COM) is the major component of urinary calculi, and its incidence is approximately 2 times as high as that of calcium oxalate dihydrate (COD) stones.[3] COM crystals are more likely to cause damage to renal tubular epithelial cells than COD crystals.[4]

The damage of renal tubular epithelial cells and the interaction between crystals and cells are important processes in stone formation.[5] CaOx crystals that adhere to the cell surface can be endocytosed into cells under the action of microvilli within 30 min.[6] Then, the endocytosed crystals are transferred to the lysosome and dissolved under the action of numerous hydrolytic enzymes to release Ca^{2+} and Ox^{2-} ions.

Received: November 27, 2022
Accepted: February 8, 2023
Published: February 20, 2023

The endocytosed crystals can directly interact with intracellular organelles, causing cell damage.[7] Studies have shown that the cytotoxicity of CaOx crystals positively correlates with the amount of endocytosed crystals.[8] Wu et al.[9] found that calcified nanoparticles can enter human kidney proximal tubular epithelial (HK-2) cells through phagocytosis, increasing the autophagy, apoptosis rate, and reactive oxygen species (ROS) levels, while decreasing the mitochondrial membrane potential. Cell damage promotes the expression of crystal adhesion molecules, such as osteopontin, transmembrane receptor protein, and hyaluronic acid, aggravating crystal adhesion and aggregation and increasing the risk of stone formation.[10]

Modulation of CaOx crystallization has long been proposed as a common therapeutic modality. A wide range of candidate molecules has been explored, from various small molecules, such as citrate derivatives or polyphosphates,[11,12] to macromolecules, including amino acids, peptides, and synthetic polymers bearing anionic functional groups.[13−17] However, most reports have focused on the effect of molecules on crystallization, ignoring their ability to regulate crystal−cell interactions. At present, the drugs used in the clinical treatment of kidney stone disease primarily include thiazide diuretics and citrate.[18] Existing medical methods have significantly reduced the recurrence rates of stones, but none can completely stop stone formation. Plant polysaccharides are rich in anionic groups. They exhibit good capability to chelate calcium ions and protect cells and good potential for inhibiting the formation and recurrence of kidney stones. Cai et al.[19] found that *Crassostrea hongkongensis* polysaccharide pre-protection can effectively improve the resistance to H_2O_2-induced oxidative damage of the intestinal epithelial cell line (IEC-6), increase the cell viability, and significantly reduce the release of intracellular ROS. Wang et al.[20] determined that *Hizikia fusiforme* polysaccharide (HFPS) can protect monkey kidney cells (Vero) against oxidative stress induced by H_2O_2. HFPS can inhibit the increase in intracellular ROS levels, improve the cell viability, and reduce the number of apoptotic cells.

Natural extracts from plants have good biocompatibility and safety and are more amenable to clinical application. Purification and modification through natural extracts are important directions in the search for stone-inhibiting drugs. Urinary levels of glycosaminoglycans are an important indicator for assessing the risk of stone formation. Lower urinary glycosaminoglycan levels are more common in patients with stone formation.[21] Seaweed polysaccharides are usually acidic mucopolysaccharides containing a high number of sulfonic acid groups, and their structure has greater similarity to that of urinary glycosaminoglycans. It has been shown that semisynthetic sulfated polysaccharides have better crystallization inhibition than naturally occurring glycosaminoglycans.[22] *Laminaria* is a genus of brown algae, and it is a plant belonging to the Macrophyllaceae family. *Laminaria* is mostly cultivated in East Asian countries, such as China, Korea, and Japan. It is a food item with high nutritional value and certain medicinal value.[23] Polysaccharide is one of the most important active ingredients of *Laminaria*; it exhibits good antioxidant activity and cell protection capability. Li et al.[24] reported that low-molecular-weight *Laminaria* polysaccharide (LP) exerts significant protective effect on acute kidney injury in rats caused by glycerol. Its protective mechanism was determined to be related to the anti-inflammatory and antioxidant effects of LP. LP can also improve the ability of mice to resist oxidative stress; increase the levels of superoxide dismutase, glutathione peroxidase, and catalase in the serum, liver, and muscles; and reduce the release of malondialdehyde.[25] In addition, LP is an anionic polysaccharide that is rich in sulfonic acid groups, which can be adsorbed onto the surface of crystals and exhibit the potential to inhibit crystal adhesion and endocytosis.

We previously extracted the original LP (LP0, with an $-OSO_3^-$ content of 0.73%) by using a hot water extraction method. LP0 is composed of maltose, glucose, raffinose, fructose, and sucrose, with the mass ratio of 12:1.4:0.09:0.08:0.03. The original LP0 was sulfated using the sulfur trioxide−pyridine method, and three sulfated LPs (SLPs) were obtained: SLP1, SLP2, and SLP3. Their sulfated ($-OSO_3^-$) contents were 15, 23, and 31%, respectively. The sulfonation modification of LP0 enhances its crystallization regulation effect on CaOx crystals and inhibits the formation of COM crystals, the crystal form with high risk for kidney stone formation.[26] The current study aims to study the protective effects of SLPs with different degrees of sulfonation on HK-2 cells and the inhibition of endocytosis of nano-COM crystals to determine the relationship between the content of sulfonic acid groups and the biological activity of polysaccharides, providing clarification for further development of drugs that can prevent and treat kidney stones.

2. MATERIALS AND METHODS

2.1. Reagents and Apparatuses. Reagents: DMEM/F-12 culture medium and fetal bovine serum were purchased from Gibco. The CCK-8 kit was purchased from Dojindo Laboratory (Kumamoto, Japan). Cell membrane red fluorescent probe 1,1′-dioctadecyl-3,3,3′,3′-tetramethylindocarbocyanine perchlorate (DiI), 4,6-diamidino-2-phenylindole (DAPI) staining solution, and Fluo-4 AM were purchased from Shanghai Biyuntian Biotechnology Co., Ltd. Annexin V-FITC/propidium iodide (PI), 5,5′,6,6′-tetrachloro-1,1′,3,3′-tetraethylbenzimi-dazolylcarbocyanine iodide (JC-1), and 2′,7-dichlorodihydrofluorescein diacetate (DCFH-DA) were purchased from KeyGEN BioTECH Co. Ltd. (Nanjing, China). Acridine orange (AO) and monodansylcadaverine (MDC) were purchased from Beijing Solarbio Technology Co., Ltd. Human kidney proximal tubular epithelial (HK-2) cells were purchased from the Shanghai Cell Bank of the Chinese Academy of Sciences (Shanghai, China).

Instruments: multifunctional microplate reader (SafireZ, Tecan, Switzerland); flow cytometer (FACS Aria, BD, USA); inverted fluorescence microscope (OLYMPUS, U-HGLGPS, Japan); laser confocal microscope (LSM510 META DUO SCAN, ZEISS, Germany); and optical microscope (OLYMPUS, TH4-200, Japan).

2.2. Experimental Methods. *2.2.1. Preparation and Characterization of Calcium Oxalate Crystals.* Nano-sized COM crystals were synthesized according to the methods used in a previous study.[27] $CaCl_2$ and K_2Ox solutions were prepared with the concentration of 0.6 mol/L in pure water. A 50 mL aliquot of each solution was directly mixed at 25 °C. The reaction mixture was stirred with a magnetic stirrer (1250 rpm) for 6 min, then ethylene glycol was added to promote the precipitation, followed by washing twice with anhydrous ethanol under ultrasonication. The crystals were collected by suction filtration and dried in a drying oven for 24 h. The prepared crystals were characterized by scanning electron

https://doi.org/10.1021/acsomega.2c07584
ACS Omega 2023, 8, 7816−7828

microscopy (SEM) and Fourier transform infrared (FT-IR) spectroscopy. The diameter of the prepared crystals was statistically measured by using Nano Measurer software (v1.2.5).

2.2.2. Extraction and Sulfation of Laminaria Polysaccharides. The extraction and sulfation of SLPs were performed with reference to our previous work.[26] The SLPs were extracted by the hot water extraction method, and the sulfur trioxide−pyridine method was used for sulfation.

The $-OSO_3H$ group content of SLPs was measured by the $BaCl_2$-gelatin turbidity method.[28] 70 mg sample of polysaccharide was placed in 10.0 mL of a 1.0 mol/L hydrochloric acid solution and then hydrolyzed at 100 °C for 6 h. 0.3% gelatin solution was prepared in hot water (60−70 °C) and stored overnight at 4 °C. 2.0 g of $BaCl_2$ was dissolved in the gelatin solution and left at room temperature for 3 h. 0.2 mL of SLP solution at a concentration of 1.4 mg/mL was added to 1 mL of $BaCl_2$-gelatin reagent and 3.8 mL of 0.5 mol/L hydrochloric acid; then, the mixture was left at 25 °C for 15 min. A blank was prepared by replacing the SLP solution with 0.2 mL of water. The released $BaSO_4$ suspension was measured at λ = 360 nm using a UV−vis spectrophotometer with K_2SO_4 as the standard, and the regression equation was $Y = 4.73X + 0.017$, $R^2 = 0.99$, $n = 11$, from which the sulfate content of the polysaccharide could be calculated.

2.2.3. Cell Culture and Grouping. HK-2 cells were cultured in DMEM/F-12 medium containing 10% fetal bovine serum in an incubator at 37 °C and 5% CO_2-saturated humidity. The experimental models were divided into three groups: (A) normal control group: only serum-free medium was added; (B) nano-COM damage group: 200 μg/mL nano-COM dispersed in serum-free medium was added and co-incubated with cells for 12 h; and (C) polysaccharide protection group: a certain concentration of SLPs with different $-OSO_3^-$ contents mixed with 200 μg/mL COM crystals was added to the cells and co-incubated for 12 h.

2.2.4. Cell Viability Detection. HK-2 cells were seeded into 96-well plates at a density of 5×10^4 cells/mL (100 μL/well) and cultured overnight. 200 μg/mL nano-COM crystals with or without the protection by SLPs (LP0, SLP1, SLP2, and SLP3) with the concentrations of 20, 40, and 80 μg/mL were added and co-incubated with cells for 12 h. After reaching the treatment time, 10 μL of CCK-8 reagent was added to each well and incubated in a 37 °C incubator for 2 h. Five parallel multiple wells were set for each group. The absorbance (A) was detected using a microplate reader at 450 nm, and the cell viability was calculated.

2.2.5. Observation of Cell Morphology. HK-2 cells were seeded into six-well plates at a density of 1.0×10^5 cells/mL and cultured overnight. 200 μg/mL nano-COM crystals with or without the protection by 80 μg/mL SLPs (LP0, SLP1, SLP2, and SLP3) were added and co-incubated with cells for 12 h. After reaching the treatment time, cell morphology was observed under an ordinary optical microscope.

2.2.6. Detection of ROS Level. 200 μg/mL nano-COM crystals with or without the protection by 80 μg/mL SLPs (LP0, SLP1, SLP2, and SLP3) were added and co-incubated with cells for 12 h. After reaching the treatment time, the supernatant was aspirated in a culture plate, 1 mL of DCFH-DA diluent was added to each well, incubated in a 37 °C incubator in the dark for 30 min, washed with serum-free medium three times, and observed with an inverted fluorescence microscope. ImageJ software was used to perform fluorescence semi-quantitative analysis.

2.2.7. Detection of Mitochondrial Membrane Potential (ΔΨm). 200 μg/mL nano-COM crystals with or without protection by 80 μg/mL SLPs (LP0, SLP1, SLP2, and SLP3) were added and co-incubated with cells for 12 h. After reaching the treatment time, the supernatant was aspirated in a culture plate, 1 mL of JC-1 working solution with a concentration of 20 μmol/L was added, incubated in a 37 °C incubator in the dark for 30 min, washed twice with PBS, and observed with an inverted fluorescence microscope. ImageJ software was used to perform fluorescence semi-quantitative analysis.

2.2.8. Detection of Lysosome Integrity. The cells were stained with 5 μg/mL AO prepared in DMEM for 15 min and washed three times with PBS. 200 μg/mL nano-COM crystals with or without protection by 80 μg/mL SLPs (LP0, SLP1, SLP2, and SLP3) were added and co-incubated with cells for 12 h. After reaching the treatment time, the mixture was washed three times with PBS and observed under a fluorescence microscope. ImageJ software was used for fluorescence semi-quantitative analysis of AO. Lysosome integrity = red light intensity/green light intensity; lysosome integrity of the treatment group = (red light intensity/green light intensity)/control lysosome integrity.

2.2.9. Detection of Intracellular Ca^{2+} Level. 200 μg/mL nano-COM crystals with or without the protection by 80 μg/mL SLPs (LP0, SLP1, SLP2, and SLP3) were added and co-incubated with cells for 12 h. After reaching the treatment time, trypsin digestion and centrifugation were done to obtain cell pellets. 200 μL of Fluo-4 AM (5 μmol/L) was added and incubated at 37 °C for 30 min. The mixture was washed with PBS three times, and detection was carried out by a flow cytometer.

2.2.10. Autophagy Detection. 200 μg/mL nano-COM crystals with or without the protection by 80 μg/mL SLPs (LP0, SLP1, SLP2, and SLP3) were added and co-incubated with cells for 12 h. After reaching the treatment time, the culture solution was removed, an appropriate amount of 1× wash buffer was added to wash twice, 1 mL of 10% MDC dye was added to each well, followed by incubating in an incubator in the dark for 30 min, and washed twice with wash buffer; autophagy fluorescence was observed with a fluorescence microscope. ImageJ software was used for fluorescence semi-quantitative analysis.

2.2.11. Detection of Cell Healing Ability. 200 μg/mL nano-COM crystals with or without the protection by 80 μg/mL SLPs (LP0, SLP1, SLP2, and SLP3) were added and co-incubated with cells for 12 h. After reaching the treatment time, the culture solution was aspirated, and a sterile 200 μL pipet tip was used to draw a line in the culture plate in a certain direction. The mixture was washed twice with PBS, and fresh medium was added to continue culturing; the change of the scratch spacing was observed under an optical microscope at regular intervals, pictures were taken, and the healing rate of the cells was calculated.

2.2.12. Apoptosis and Necrosis Detection. 200 μg/mL nano-COM crystals with or without the protection by 80 μg/mL SLPs (LP0, SLP1, SLP2, and SLP3) were added and co-incubated with cells for 12 h. After reaching the treatment time, the mixture was washed twice with PBS solution, trypsinized, the cells were collected and suspended, and then centrifuged (1000 rpm, 5 min) to obtain cell pellets. 200 μL of binding buffer was added, mixed well, then 5 μL of Annexin V-

https://doi.org/10.1021/acsomega.2c07584
ACS Omega 2023, 8, 7816−7828

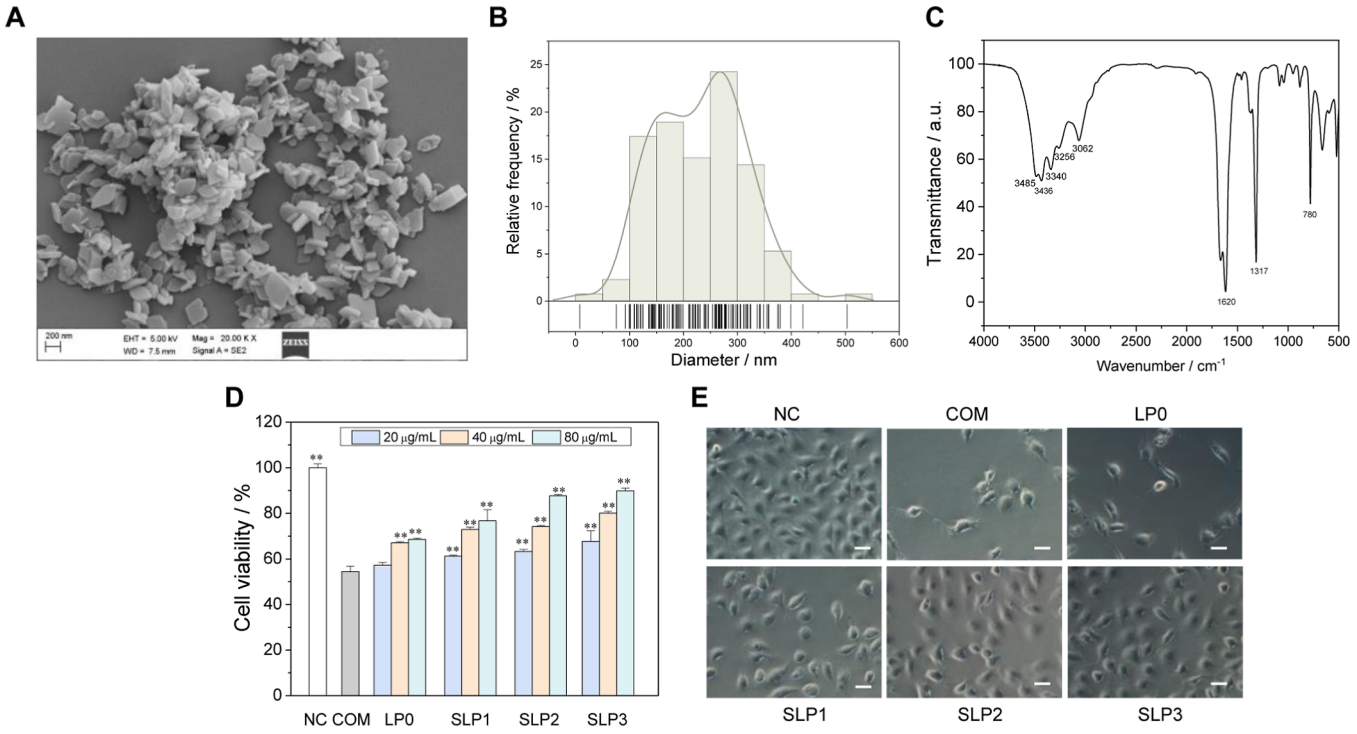

Figure 1. Characterization of nano-COM crystals. (A) SEM images, (B) particle size distribution, and (C) FT-IR spectra of nano-COM crystals. The changes of (D) cell viability and (E) cell morphology of HK-2 cells after treatment of nano-COM crystals with or without protection by SLPs (LP0, SLP1, SLP2, and SLP3) for 12 h. COM concentration: 200 μg/mL. SLP concentrations: 20, 40, and 80 μg/mL. Scale bars: 200 nm (SEM images); 50 μm (ordinary light microscopy images). Compared with the COM treatment group, $^{*}P < 0.05$, $^{**}P < 0.01$.

FITC was added, followed by incubation for 10 min at room temperature in the dark. The mixture was centrifuged and the supernatant removed. 200 μL of binding buffer was added, mixed well, then 5 μL of PI staining solution was added, and detection was carried out by flow cytometry.

2.2.13. Fluorescent Labeling of COM Crystals. According to our previous study,[29] the nano-COM was labeled with FITC. First, 5 mL of aminopropyltriethoxysilane (AMPTES) was reacted with COM (0.05 g) and absolute ethanol (50 mL) at 74 °C for 3 h. Subsequently, 0.025 g of FITC was supplemented, and the reaction was maintained for 6 h. Fluorescence-labeled COM were harvested followed by washing and drying.

2.2.14. Quantitative Detection of the Proportion of Cells with Endocytosed Crystals. 200 μg/mL FITC-labeled nano-COM crystals with or without the protection by 80 μg/mL SLPs (LP0, SLP1, SLP2, and SLP3) were added and co-incubated with cells for 12 h. After reaching the treatment time, the culture medium was aspirated into a six-well plate, washed twice with PBS, and treated with EDTA (5 mM) for 10 min to remove the adherent crystals. After trypsinization, the cells were resuspended in PBS, and the proportion of fluorescent cells was detected by flow cytometry.

2.2.15. Qualitative Observation of Crystal Endocytosis by Confocal Microscopy. 200 μg/mL FITC-labeled nano-COM crystals with or without the protection by 80 μg/mL SLPs (LP0, SLP1, SLP2, and SLP3) were added and co-incubated with cells for 12 h. After reaching the treatment time, the mixture was washed twice with PBS and treated with EDTA (5 mM) for 10 min; the adherent crystals were removed, the cell membrane was stained with DiI for 20 min, the cell nucleus was stained with DAPI for 10 min, and fixed with 4% paraformaldehyde for 10 min. Endocytosis of crystals in the cells was observed using confocal microscopy. The internalized crystals were observed by confocal observation.

2.2.16. Statistical Analysis. Statistical analyses were performed using the SPSS 13.0 software. Data were expressed as mean ± SD. Multiple group comparisons were performed using one-way ANOVA, followed by the Tukey post hoc test. If $p < 0.05$, there was significant difference; if $p < 0.01$, the difference was extremely significant; if $p > 0.05$, there was no significant difference.

3. RESULTS

3.1. SLPs Improve Cell Viability. The SEM image of the calcium oxalate crystal is shown in Figure 1A. The crystals had a rhombic shape. The diameter of the prepared crystals was statistically measured to be approximately 230 ± 80 nm by using Nano Measurer software (v1.2.5) (Figure 1B). The FT-IR spectra of the calcium oxalate crystals showed a broad band, which corresponds to the symmetric and asymmetric stretching vibration peaks of the O−H bond of crystal water at 3485−3062 cm^{-1}, and split into five absorption peaks, which were the characteristic peaks of COM (Figure 1C).[30] The asymmetric (ν_{as}) and symmetric stretching vibrations (ν_{s}) of the carboxyl group (−COO) in COM were at about 1620 and 1317 cm^{-1}, respectively.

Normal cells were damaged by 200 μg/mL of the prepared nano-sized COM crystals in 12 h, and the cell viability decreased to 54% (Figure 1D, $p < 0.01$). After being protected by SLPs with different sulfonation degrees, cell viability gradually increased with an increase in SLP concentration and sulfonic acid group content. At a concentration of 80 μg/mL, the protected cell viability of the four SLPs was 68% (LP0), 76% (SLP1), 88% (SLP2), and 90% (SLP3).

https://doi.org/10.1021/acsomega.2c07584
ACS Omega 2023, 8, 7816−7828

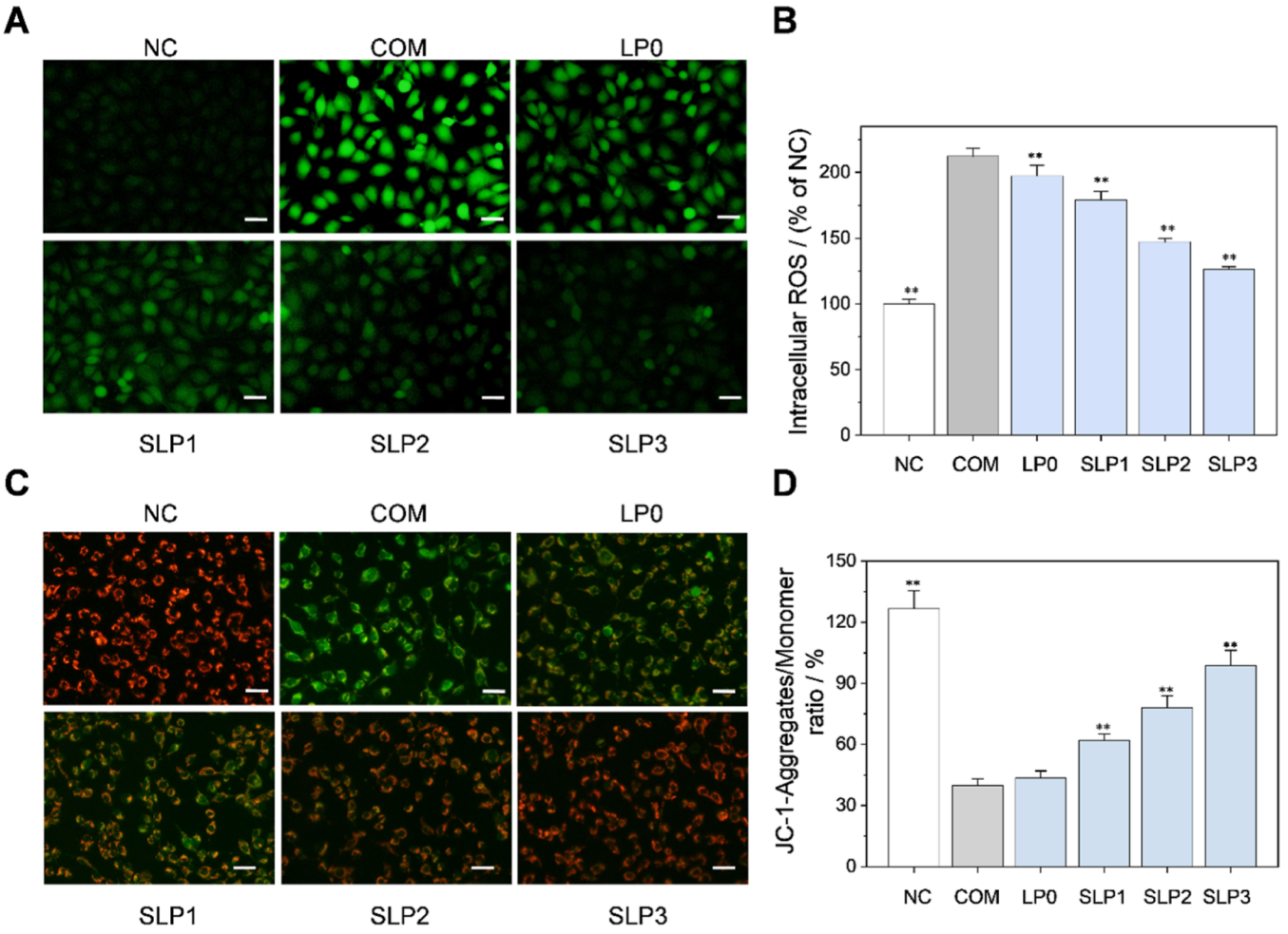

Figure 2. Changes of reactive oxygen (ROS) and mitochondrial membrane potential (ΔΨm) of HK-2 cells after treatment of nano-COM crystals with or without protection by SLPs (LP0, SLP1, SLP2, and SLP3) for 12 h. (A) ROS distribution observed by a fluorescence microscope; (B) quantitative detection of fluorescence intensity of ROS; (C) visualization of ΔΨm; and (D) quantitative result of ΔΨm. COM concentration: 200 μg/mL. SLP concentration: 80 μg/mL. Scale bars: 50 μm. Compared with the COM treatment group, $^{*}P < 0.05$, $^{**}P < 0.01$.

3.2. SLPs Restore Cell Morphology. The morphological changes of SLP-protected and SLP-unprotected nano-COM-treated cells were observed under a light microscope (Figure 1E). In the normal group, cell morphology remained intact, showing a spindle-shaped morphology, and the cell-to-cell connection was tight. After the cells were treated with nano-COM crystals, cell density was evidently reduced and cell morphology was disordered. Under the protection of SLPs, the damage caused by COM crystals to the cells was reduced. The cell density of the protected group was higher than that of the COM-injured group, and cell morphology was restored to varying degrees. The SLP3 group improved the most.

3.3. SLPs Reduce Intracellular ROS Levels. Intracellular ROS was fluorescently labeled with dichlorodihydrofluorescein diacetate and observed under a fluorescence microscope (Figure 2A). The green fluorescence of normal cells was extremely weak, indicating that their ROS levels were low. Meanwhile, the ROS levels in the COM-damaged group were significantly increased ($p < 0.01$, Figure 2B). After adding the four types of SLPs for protection, the fluorescence intensity of all ROS levels decreased to varying degrees, indicating that the SLPs can protect cells from COM crystal damage, with SLP3, which had the highest $-OSO_3^-$ content, exhibiting the best protective capability (Figure 2B).

3.4. SLPs Increase Mitochondrial Membrane Potential (ΔΨm). We used the fluorescent dye JC-1 to label the intracellular mitochondrial membrane potential and observed the changes of ΔΨm in SLP-protected and SLP-unprotected cells damaged by COM crystals via fluorescence microscopy (Figure 2C). In normal cells, ΔΨm was in a high potential state, which mostly produced red fluorescence. After COM damage, ΔΨm decreased, mostly emitting green fluorescence. Under the protection of SLPs, the intensity of red fluorescence gradually increased with an increase in sulfonic acid group content, indicating that ΔΨm gradually increased. SLPs restored the polarity state of membrane potential.

3.5. SLPs Improve Lysosome Integrity. AO emits red fluorescence in lysosomes and green fluorescence in cytoplasm. The intensity of red fluorescence can indicate the quality of lysosome integrity. Normal cells emitted strong red fluorescence. When lysosomal integrity was damaged, the intensity of red fluorescence decreased. We used a fluorescence microscope to observe the changes in lysosomal integrity of HK-2 cells caused by COM under SLP-protected or -unprotected conditions. The lysosome structure of the cells in the normal group was complete, and red fluorescence and green fluorescence were superimposed to display a more orange-red fluorescence (Figure 3A). The lysosomal integrity

https://doi.org/10.1021/acsomega.2c07584
ACS Omega 2023, 8, 7816−7828

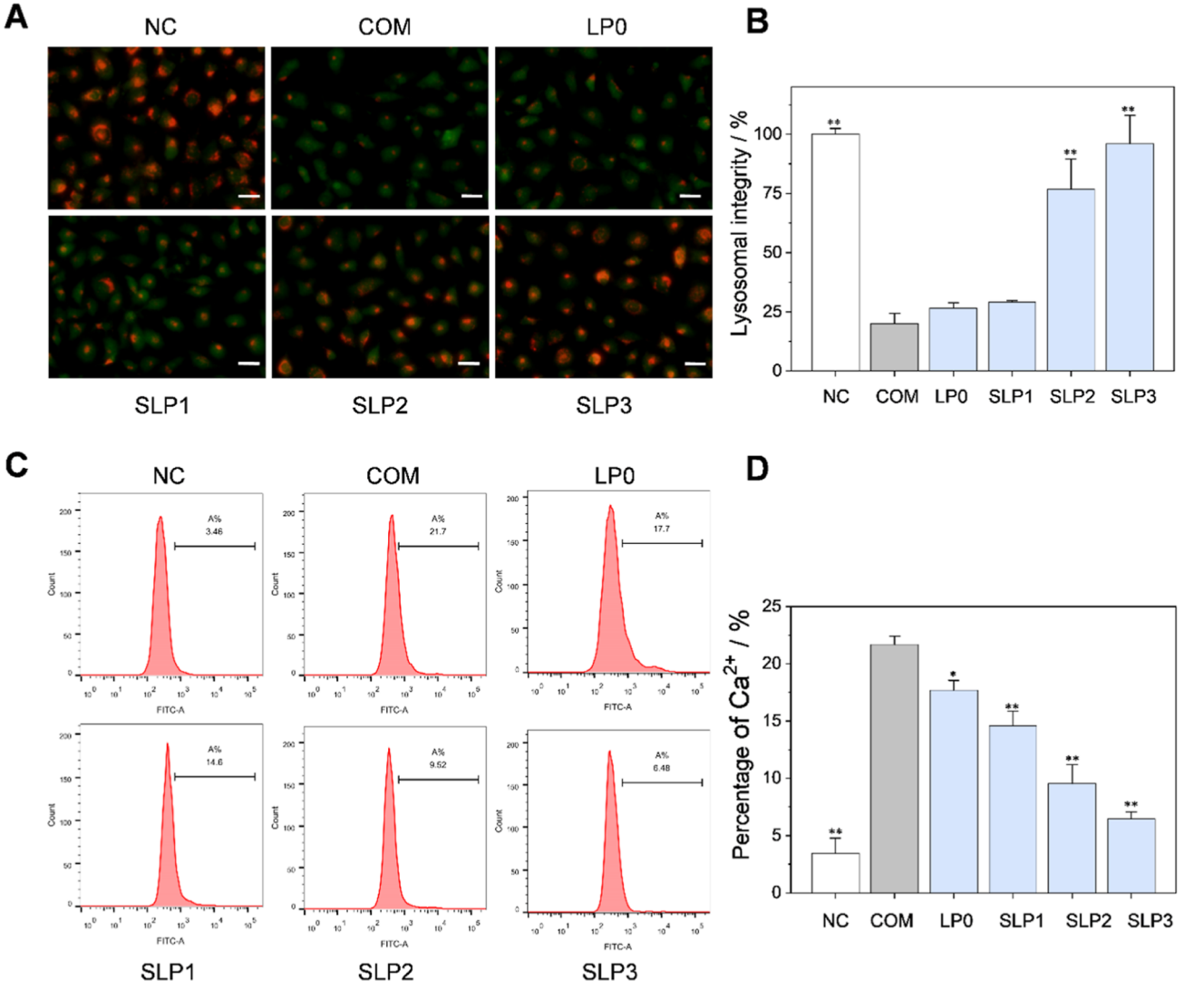

Figure 3. Changes of lysosomal integrity and intracellular Ca^{2+} levels of HK-2 cells after the treatment of nano-COM crystals with or without the protection by SLPs (LP0, SLP1, SLP2, and SLP3) for 12 h. (A) Lysosomal integrity was observed by fluorescence microscopy; (B) quantitative histogram of lysosomal integrity; (C) intracellular Ca^{2+} levels detected by flow cytometry; and (D) quantitative histogram of Ca^{2+} levels. COM concentration: 200 μg/mL. SLP concentration: 80 μg/mL. Scale bars: 50 μm. Compared with the COM treatment group, $^{*}P < 0.05$, $^{**}P < 0.01$.

of the cells was destroyed after COM crystal damage, and red fluorescence was evidently weakened. SLPs can improve the lysosomal integrity, with SLP3, which had the highest $-OSO_3^-$ content, demonstrating the best ability to inhibit COM damage in cells (Figure 3B).

3.6. SLPs Reduce Intracellular Ca^{2+} Levels. We used a Fluo-4 AM fluorescent probe to label intracellular Ca^{2+} and flow cytometry to detect the level of Ca^{2+} (Figures 3C,D). Compared with that in the normal group, the intracellular Ca^{2+} level rose from 3.5 to 22% ($p < 0.01$) in the COM crystal-damaged group. Under the protection of SLPs, the cellular Ca^{2+} level evidently decreased (6.5−18%) and Ca^{2+} level decreased with an increase in the $-OSO_3^-$ content of SLPs. The level of Ca^{2+} in the SLP3-protected group, which had the highest $-OSO_3^-$ content, was the closest to the level of normal cells.

3.7. SLPs Regulate Autophagy. We used MDC to label intracellular autophagic vacuoles fluorescently and observed the autophagy fluorescence intensity of SLP-protected and SLP-unprotected cells under a fluorescence microscope (Figure 4A,B). The cells in the normal group emitted weak blue fluorescence, while the COM crystal-damaged group displayed strong blue fluorescence. That is, a large number of autophagic vacuoles appeared, indicating that crystal damage promoted autophagy activity. Under the protection of SLPs, the intensity of blue fluorescence decreased. That is, autophagy vacuoles were evidently reduced, and the blue fluorescence intensity of the SLP3-protected group decreased the most and was closest to the normal group.

The autophagy levels of SLP-protected and SLP-unprotected cells were quantitatively detected via flow cytometry (Figure 4C,D). The order of autophagy levels from high to low was as follows: COM group > LP0 group > SLP1 group > SLP2 group > SLP3 group > normal group. This result indicates that each SLP-protected group can inhibit the autophagy activity of cells, and the amount of autophagy is negatively correlated with the content of polysaccharide $-OSO_3^-$.

3.8. SLPs Improve Cell Healing Capability. We observed the healing capability of SLP-protected and SLP-

https://doi.org/10.1021/acsomega.2c07584
ACS Omega 2023, 8, 7816−7828

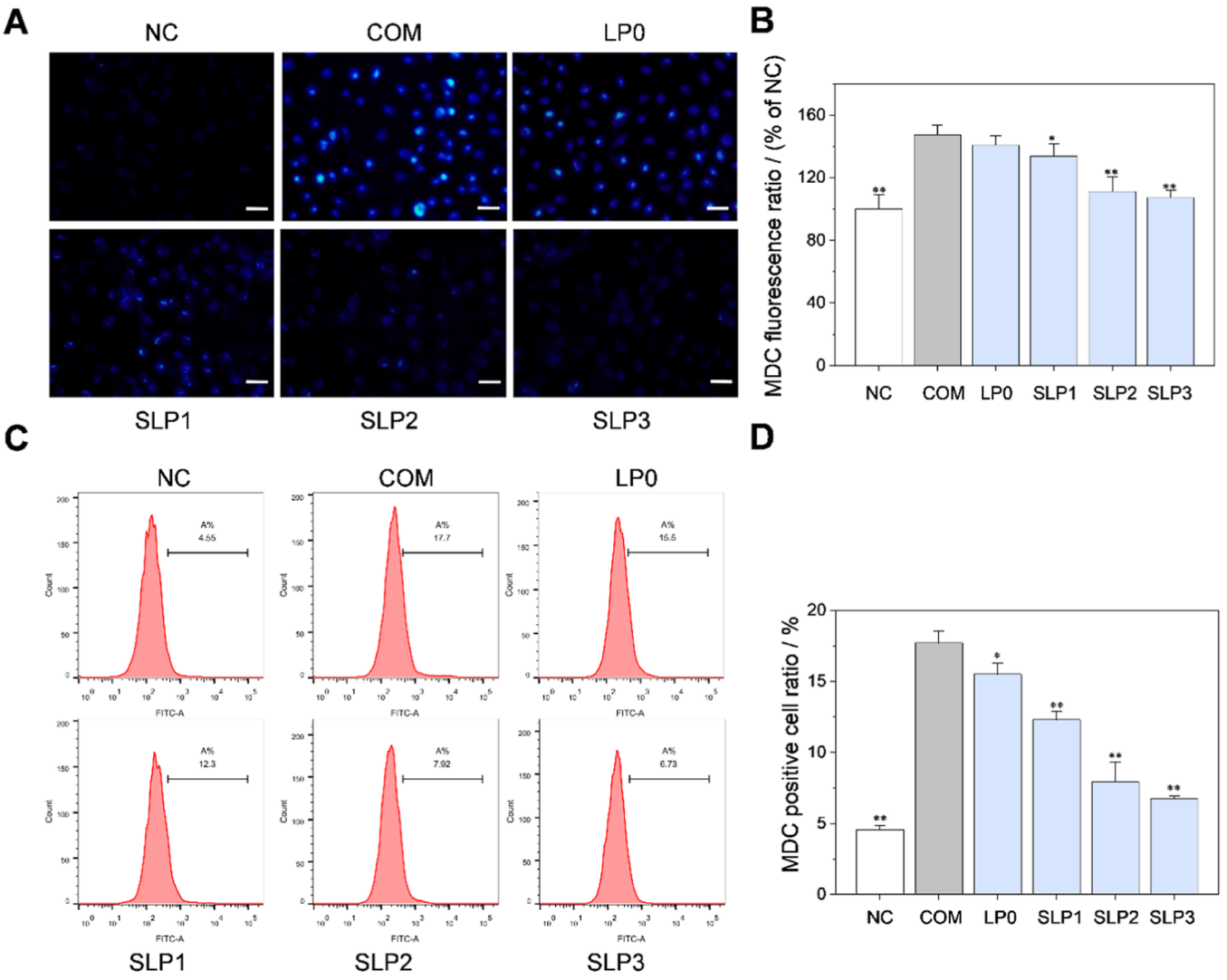

Figure 4. SLPs inhibit autophagy of nano-COM treated cells. (A) Fluorescence microscopy image; (B) quantitative histogram of MDC fluorescence intensity; (C) flow cytometry quantitative detection of autophagy level; and (D) quantitative histogram of autophagy levels. COM concentration: 200 μg/mL. SLP concentration: 80 μg/mL. Protection time: 12 h. Magnification: 400×. Scale: 50 μm. Compared with the COM treatment group, $^{*}P < 0.05$, $^{**}P < 0.01$.

unprotected cells under an ordinary microscope (Figure 5). With the extension of culture time, the number of cells in the scratches of the normal group increased evidently, the cells grew rapidly close to healing, and the healing rate was the fastest (30 $\mu m \cdot h^{-1}$). The healing rate of cells in the COM-injured group was the slowest (18 $\mu m \cdot h^{-1}$). Under the protection of SLPs, the number of cells at the scratches and the healing rate increased to varying degrees (20−27 $\mu m \cdot h^{-1}$, Figure 5A−C). The higher the $-OSO_3^-$ content of an SLP, the more it can promote the rapid healing of scratches.

3.9. SLPs Inhibit Cell Death. The cells were fluorescently labeled with Annexin V/PI, and the ratio of apoptosis and necrosis of cells was detected via flow cytometry (Figure 6A,B). The necrosis rate (Q1 + Q2) of cells in the normal group was 2.0%, and the apoptosis rate (Q3) was 1.4%. The necrosis and apoptosis rates of the COM-injured group were 22 and 2.5%, respectively. Under the protection of SLPs, the cell necrosis rate caused by COM was significantly lower than that of the COM group without SLP protection ($p < 0.01$). The cell necrosis rates of the LP0-, SLP1-, SLP2-, and SLP3-protected groups were 18, 14, 12, and 7.4%, respectively. The apoptosis rate of each SLP-protected group did not change considerably (1.1−2.0%). COM damage largely induced the necrosis of HK-2 cells, and SLPs can effectively inhibit the necrosis rate of cells.

3.10. SLPs Inhibit the Endocytosis of Nano-COM Crystals. Nano-COM was fluorescently labeled with fluorescein isothiocyanate (FITC), and the proportion of FITC-positive cells was detected via flow cytometry (Figure 6C,D). The adhered COM crystals were removed via complexation and dissolution with ethylenediaminetetraacetic acid. The detected FITC-positive cells were cells with internalized crystals. In the group without SLP protection, the percentage of cells with endocytosed COM crystals was 48%. After SLP protection, the percentage of cells with endocytosed crystals decreased to varying degrees. The percentage of cells with endocytosed COM crystals was ordered as follows: LP0 (33%) > SLP1 (24%) > SLP2 (18%) > SLP3 (6.7%). The protective effect of SLPs was positively correlated with the $-OSO_3^-$ content of polysaccharides.

In addition, we observed the endocytosis of nano-COM crystals by HK-2 cells through confocal microscopy (Figure

https://doi.org/10.1021/acsomega.2c07584
ACS Omega 2023, 8, 7816−7828

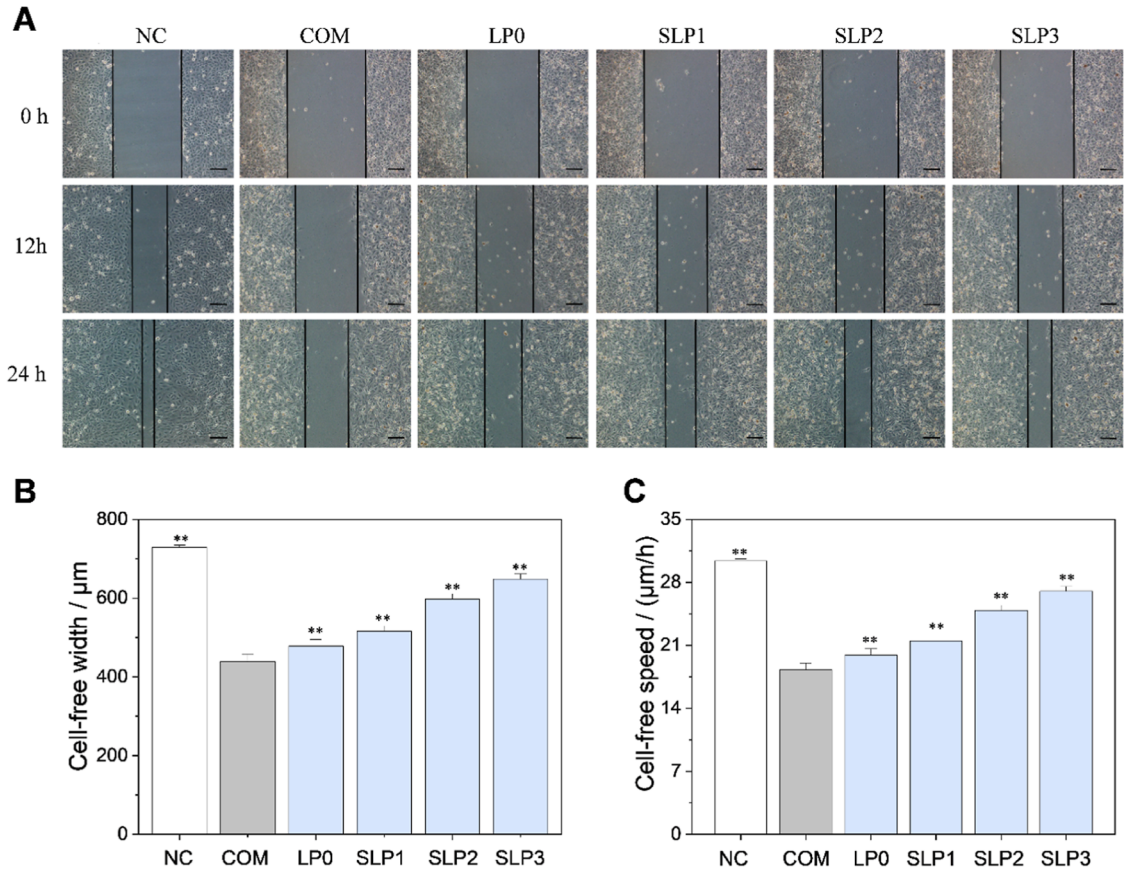

Figure 5. SLPs improved cell healing of nano-COM-treated cells. (A) Cell healing observation under an ordinary microscope; (B) quantitative histogram of cell-free width; and (C) quantitative histogram of cell healing rate. COM concentration: 200 μg/mL. SLP concentration: 80 μg/mL. Protection time: 12 h. Scale bars: 200 μm. Compared with the COM treatment group, $^{*}P < 0.05$, $^{**}P < 0.01$.

7A) and calculated FITC green fluorescence (Figure 7B). FITC-labeled COM crystals emitted green fluorescence, DiI-stained cell membranes showed red fluorescence, and DAPI-stained cell nuclei exhibited blue fluorescence. More crystals were endocytosed in the COM-treated group without SLP protection. After SLP protection, the endocytosis of nano-COM was evidently reduced, and the endocytosis amount was the least after SLP3 protection. This result indicates that SLPs can prevent the endocytosis of the crystal by cells and thus protect cells from damage by the crystal. From the correlation analysis, the number of endocytosed crystals by cells is positively correlated with the cell death rate ($R^2 = 0.90$; Figure 7C).

4. DISCUSSION

4.1. Influence of the $-OSO_3^-$ Content of Polysaccharides on Their Biological Activity. The biological functions of polysaccharides are closely related to their structural characteristics, including the substitution degree of the active group, molecular weight, monosaccharide composition, and glycosidic bonds in polysaccharides. Some natural polysaccharides exhibit poor biological activity due to the low content of their functional groups, such as $-OSO_3^-$ and $-COOH$.[31] Sulfonation modification is widely used in the molecular modification of polysaccharides. This method can enhance the biological activity of an original polysaccharide while simultaneously improving its water solubility.[31,32] Gunasekaran et al.[33] modified the acidic polysaccharide fraction of *Pleurotus eous* (P3a) to obtain a sulfated derivative (SP3a). The antioxidant, anticoagulant, antitumor, and antibacterial activities of SP3a are stronger than those of P3a. Guo et al.[34] modified Qingke β-glucans (THB) by sulfation and prepared three sulfated derivatives, namely, THB-S1, THB-S2, and THB-S3, with substitution degrees of 0.25, 0.42, and 0.58, respectively. Their antioxidant activity and in vitro hypolipidemic activity are THB < THB-S1 < THB-S2 < THB-S3.

The results of the current study showed that the four SLPs with different $-OSO_3^-$ contents can protect HK-2 cells from damage caused by nano-COM crystals. With an increase in the $-OSO_3^-$ content of SLPs, their protective effect on cells against crystal damage becomes stronger. An increase in $-OSO_3^-$ content improves the antioxidant capacity of polysaccharides and better reduces cell damage caused by COM crystals. In addition, an increase in $-OSO_3^-$ content increases direct adsorption between polysaccharides and crystals, and thus, more SLPs are adsorbed onto the surface of COM crystals and inhibit the endocytosis of these crystals. A diagram of SLPs protecting HK-2 cells against nano-COM crystal damage and inhibiting crystal endocytosis is shown in Figure 8.

4.2. SLPs Inhibit Oxidative Damage Caused by Nano-COM Crystals to HK-2 Cells. Numerous studies have shown that CaOx crystals in acute hyperoxaluria originate in the proximal tubule.[35−37] Oxalate concentrations in proximal tubules are usually high. Proximal tubule cells are more sensitive than distal tubule and collecting duct cells and are more susceptible to crystalline or oxalate damage, which

https://doi.org/10.1021/acsomega.2c07584
ACS Omega 2023, 8, 7816−7828

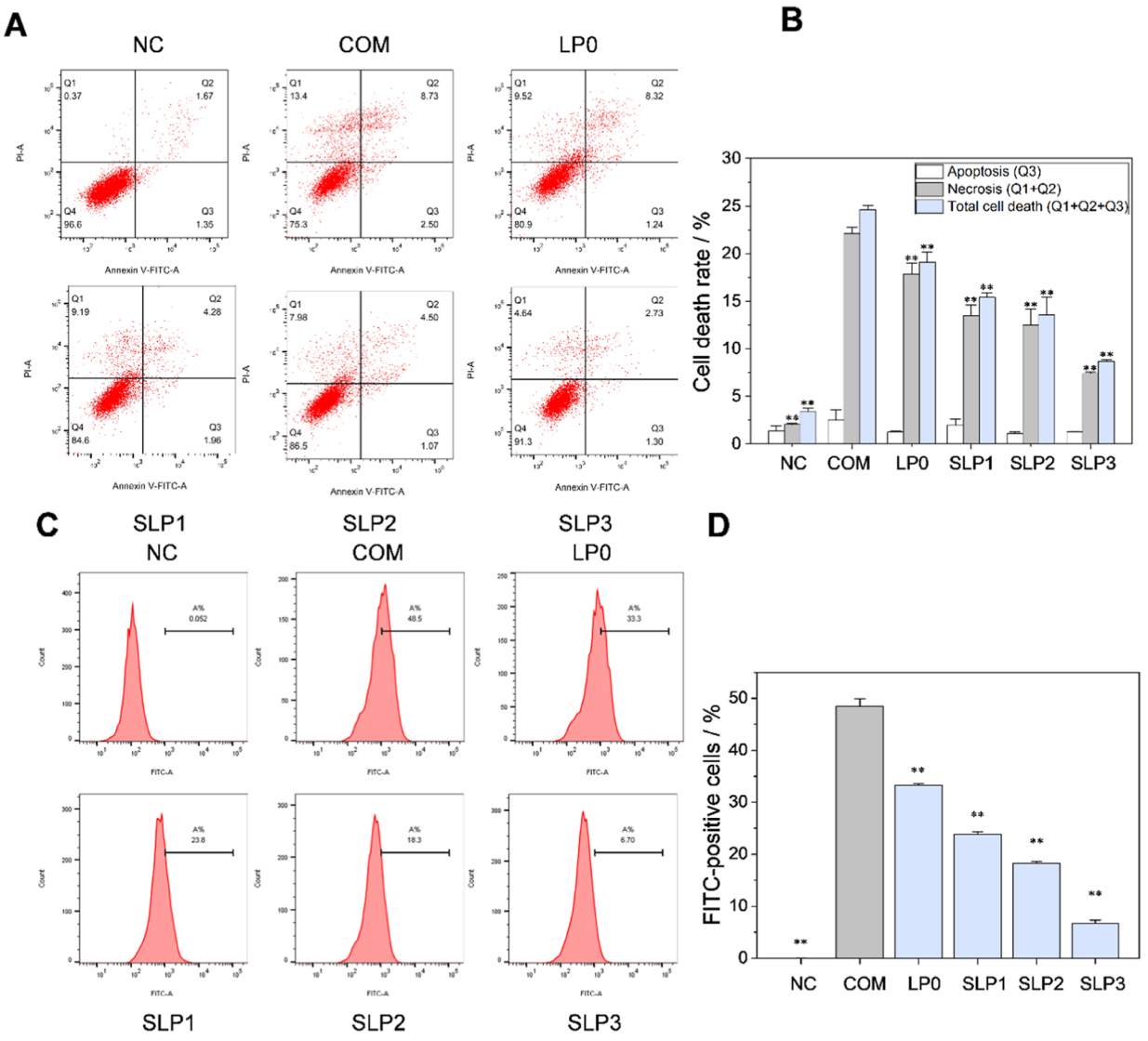

Figure 6. Changes of the cell death rate and the proportion of cells with internalized crystals after the treatment of nano-COM crystals with or without the protection by SLPs (LP0, SLP1, SLP2, and SLP3) for 12 h. (A) Quantitative detection of cell apoptosis and necrosis by Annexin V/PI double staining, quadrants Q1, Q2, Q3, and Q4 denote the ratio of necrotic cells, late-stage apoptotic and necrotic cells, early-stage apoptotic cells, and normal cells, respectively; (B) quantitative histogram of cell apoptosis and necrosis rates; (C) quantitative detection of the proportion of cells with internalized crystals by flow cytometry; and (D) quantitative histogram of the proportion of cells with internalized crystals. SLP concentration: 80 μg/mL. Protection time: 12 h. Compared with the COM treatment group, $^{**}P < 0.01$.

induces the secretion of adhesion molecules.[38] Adhesion and aggregation behavior is induced when membrane fragments and secreted adhesion molecules formed after crystal-induced injury in the upstream proximal tubule are transferred to the distal and collecting ducts. Although lithogenesis occurs in the distal parts of the nephron and renal papillae, adhesion and aggregation are primarily caused by the transfer of adhesion molecules as a result of injury to the proximal tubule.[39] Therefore, an understanding of the injury behavior of the proximal tubule is necessary. Renal epithelial cell injury is an important cause of kidney stone formation. When excessive oxalate, microcrystals, or other foreign substances cause damage beyond a cell's own repair capability, they will cause cell death.[40] To date, the available pharmacological treatments remain inadequate. In the current study, we investigated the protection activity of SLPs and evaluated their role in COM-induced HK-2 cell damage.

In addition to attaching directly to the cell membrane's surface of damage cells, nano-COM crystals can also be endocytosed into cells, further causing intracellular damage.[41] Considering the high surface area of nano-COM crystals, a large number of active sites are produced to capture oxygen molecules, leading to the generation of superoxide radicals ($\bullet O_2^-$) and other ROS through dismutation or the Fenton reaction.[41] ROS plays a key role in various signaling and pathological processes, and it is essential for human life. However, the excessive production of ROS by exogenous stimulation is harmful because ROS can induce the oxidation of DNA, proteins, or lipids, resulting in cell death.

SLPs can effectively reduce the production of ROS in cells and reduce the oxidative damage caused by COM exposure. The protective effect of SLPs on HK-2 cells is proportional to their $-OSO_3^-$ group content. As an antioxidant, polysaccharides can provide a single electron or hydrogen atom to terminate the free-radical chain reaction and achieve free-

https://doi.org/10.1021/acsomega.2c07584
ACS Omega 2023, 8, 7816−7828

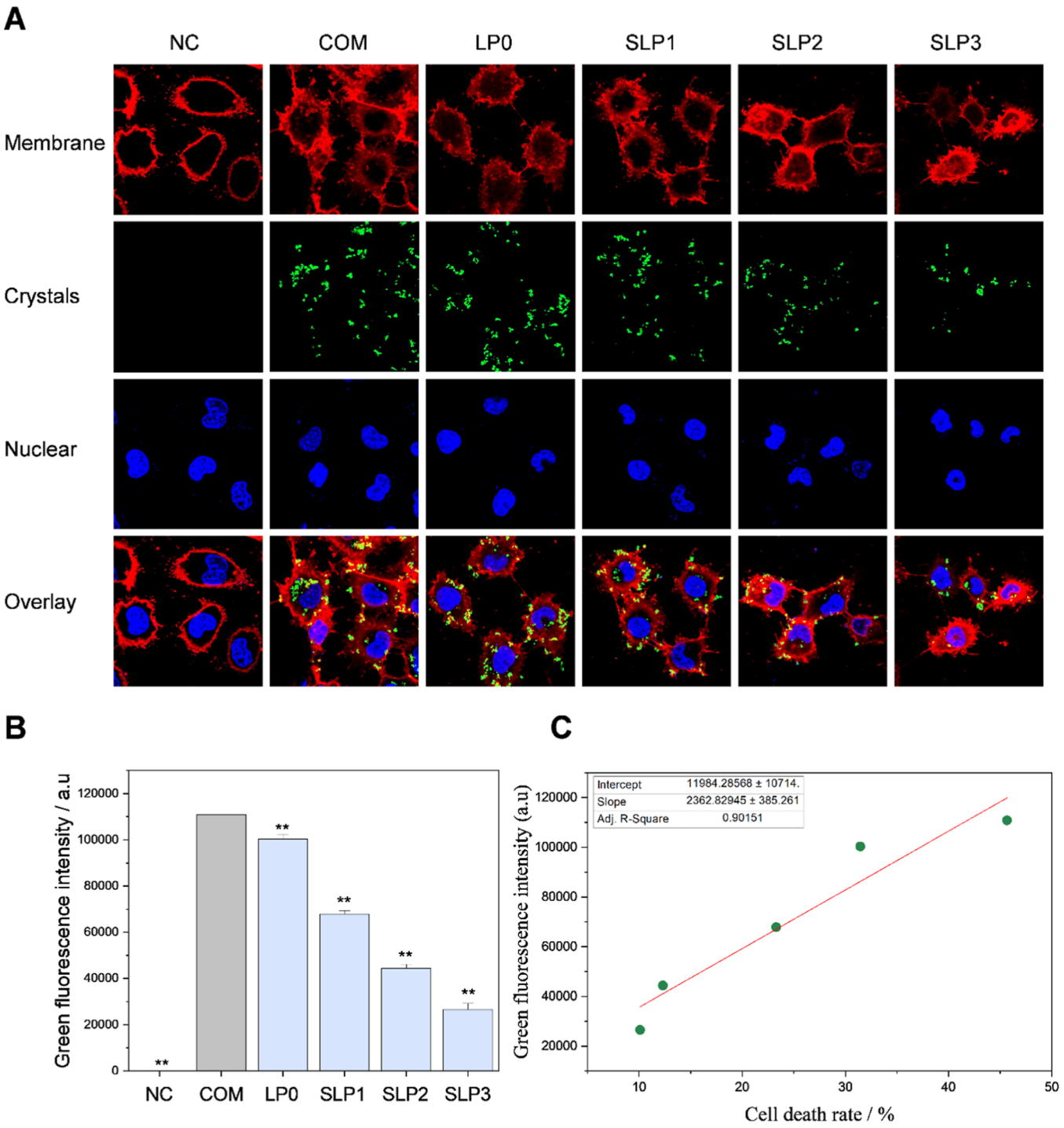

Figure 7. SLPs inhibited COM crystals endocytosis as observed by laser scanning confocal microscopy. Cell membrane (red fluorescence); nucleus (blue fluorescence); COM crystals (green fluorescence). (A) Fluorescence microscope image; (B) quantitative histogram of green fluorescence intensity; and (C) linear relationship of the proportion of cells with internalized crystals and cell death rate. R^2 is a linear correlation coefficient. SLP concentration: 80 μg/mL. Protection time: 12 h. Compared with the COM treatment group, $^*P < 0.05$, $^{**}P < 0.01$.

radical scavenging.[42] Compared with natural LP0, sulfated SLP exhibits a stronger antioxidant activity and can reduce the ROS level. The antioxidant capacity of polysaccharides is largely due to the donor capability of hydrogen atoms. Hydrogen combines with free radicals and forms stable free radicals to terminate the free-radical chain reaction. SLPs with higher $-OSO_3^-$ content demonstrate a strong capability to activate the hydrogen atoms of anomeric carbon, enhancing the donor capability of hydrogen atoms.[43]

An inseparable relationship exists between oxidative stress and mitochondrial function. Excessive ROS in the body can cause a series of damage to the mitochondrion, including depolarization of the mitochondrial membrane potential, mitochondrial DNA damage, Ca^{2+} outflow, and reduction of ATP synthesis, ultimately leading to cell death.[44] The improvement of mitochondrial function can promote aerobic respiration and reduce ROS production, reducing cell death. Wang et al.[44] determined that the polysaccharide from the

https://doi.org/10.1021/acsomega.2c07584
ACS Omega 2023, 8, 7816−7828

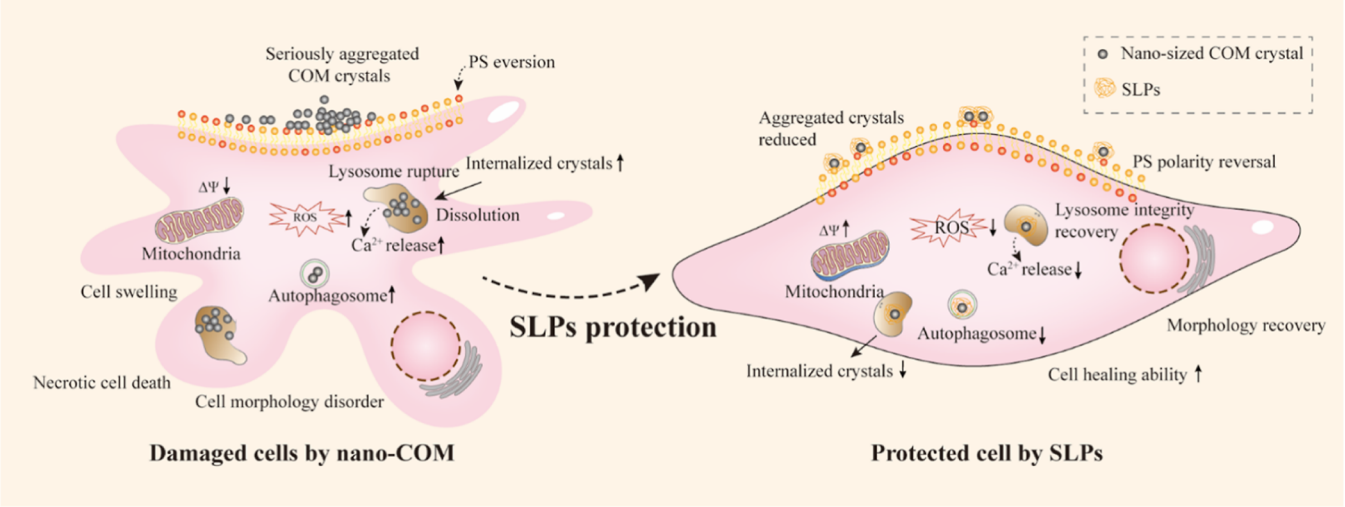

Figure 8. Proposed schematic illustration of SLPs protecting HK-2 cells against nano-COM crystal damage and inhibiting crystal endocytosis.

mycelium of *Hericium erinaceus* (EP-1) exhibits evident antioxidant activity and can protect the mitochondrion from oxidative damage. Zhang et al.[45] found that the astragalus polysaccharide can reduce ROS production and ΔΨm loss, promoting cell growth. The results of the current study show that SLPs that are rich in $-OSO_3^-$ can inhibit the decrease in ΔΨm caused by nano-COM crystals and restore the polarity of the mitochondrion (Figure 2C).

Lysosomes are important organelles for digesting foreign substances. They contain a variety of acid hydrolases and have a pH of approximately 4.5.[46] Studies have shown that endocytosed crystals are transported to the lysosome and degraded under the action of acid hydrolase. However, when the number of endocytosed crystals exceeds the capability of lysosomes to degrade, the crystals will damage the lysosomes, leading to the destruction of lysosomal integrity. The rapid rupture of lysosomes is an important cause of cell necrosis.[47] Endocytic COM is dissolved under the action of acid hydrolase and releases Ca^{2+} and Ox^{2-}. The excessive release of Ca^{2+} and Ox^{2-} will cause a serious imbalance of osmotic pressure inside and outside a cell, eventually leading to cell membrane rupture and even cell necrosis.[29] SLPs can inhibit the endocytosis of COM and reduce the release of Ca^{2+} and Ox^{2-}, reducing the damage of COM to lysosomes and improving the integrity of lysosomes.

Autophagy is a dynamic process involving the degradation of intracellular substances related to lysosomes. It can protect cells from potential damages related to stress. Polysaccharides exhibit the effect of regulating autophagy on cells. Hou et al.[48] reported that *Ganoderma atrum* polysaccharide (PSG-1) exerts a protective effect on acrolein-induced macrophage damage. PSG-1 treatment can effectively inhibit autophagy in acrolein-treated macrophages and reduce cell apoptosis. The results of the current study show that SLPs can protect HK-2 cells from oxidative damage caused by nano-COM crystals, and the protective effect is closely related to the $-OSO_3^-$ content. SLPs reduce oxidative damage caused by COM crystals and decrease the level of autophagy (Figure 7).

4.3. SLPs Inhibit the Endocytosis of COM Crystals by Cells. The adhered CaOx crystals can be endocytosed into cells within 30−60 min.[6] The internalized crystals are transferred to lysosomes via vesicular transport. The intracellular lysosome contains a variety of acid hydrolases that can dissolve the internalized COM crystals into Ca^{2+} and Ox^{2-} ions for excretion. Simultaneously, excessive internalized crystals that exceed the natural digestion capacity of a cell aggravate cell damage.[8]

The results of the current study show that compared with that in the COM-injured group, the number of endocytosed nano-COM crystals after SLP protection is evidently reduced. As the $-OSO_3^-$ content of SLPs increases, the inhibitory effect of HK-2 cells on the endocytosis of crystals is gradually enhanced. SLPs rich in $-OSO_3^-$ anionic groups can be adsorbed onto the surface of positively charged COM crystals through electrostatic interaction, increasing the negative charge on the crystal surface. The combination of crystals and polysaccharides increases the negative charge on the surface of COM crystals and the repulsion between the crystal and the negatively charged cell membrane, inhibiting crystal endocytosis.

The number of endocytosed crystals by cells is positively correlated with the cell death rate (R^2 = 0.90; Figure 7C). The excessive endocytosis of crystals is an important cause of cell damage. That is, the more crystals that are endocytosed, the greater the damage to cells. Crystal endocytosis increases the burden of the lysosome, leading to lysosome rupture. After the lysosome ruptures, Ca^{2+} and Ox^{2-} are released into the cytoplasm. The excessive release of Ca^{2+} and Ox^{2-} can cause the depolarization of the mitochondrion, resulting in the overexpression of ROS, and ultimately, cell death.

The chemically modified LPs exhibited a better reduction in calcium oxalate crystal toxicity than the natural component. However, it is not a foregone conclusion that the chemically modified LPs are more biocompatible than other synthetic chemicals. The specific anti-calculus effect and biosafety of modified polysaccharides have yet to be verified in animal and clinical data.

5. CONCLUSIONS

Four SLPs with different $-OSO_3^-$ contents exhibit protective effects on HK-2 cells. The SLPs reduce cell damage caused by nano-COM crystals, improve cell viability, restore cell morphology, reduce ROS production, improve ΔΨm and lysosome integrity, inhibit cell necrosis, and evidently constrain nano-COM crystal endocytosis. The higher the $-OSO_3^-$ content of SLPs, the stronger their capability to protect HK-

https://doi.org/10.1021/acsomega.2c07584
ACS Omega 2023, 8, 7816−7828

2 cells against nano-COM damage. Increasing the $-OSO_3^-$ content of polysaccharides may be an effective approach for improving the anti-calculus effect of polysaccharides. SLP3, which has the highest $-OSO_3^-$ content, may be used as a potential drug for preventing kidney stone formation and recurrence.

AUTHOR INFORMATION

Corresponding Author

Xin-Yuan Sun − *Department of Urology, Guangzhou Institute of Urology, Guangdong Key Laboratory of Urology, the First Affiliated Hospital of Guangzhou Medical University, Guangzhou Medical University, Guangzhou, Guangdong 510230, China;* orcid.org/0000-0002-8929-1099; Email: sunxinyuan1985@163.com

Authors

Bang-Xian Yu − *Department of Urology, Guangzhou Institute of Urology, Guangdong Key Laboratory of Urology, the First Affiliated Hospital of Guangzhou Medical University, Guangzhou Medical University, Guangzhou, Guangdong 510230, China*

Yi-Han Zhang − *Department of Urology, Guangzhou Institute of Urology, Guangdong Key Laboratory of Urology, the First Affiliated Hospital of Guangzhou Medical University, Guangzhou Medical University, Guangzhou, Guangdong 510230, China*

Chun-Yao Li − *Department of Urology, Guangzhou Institute of Urology, Guangdong Key Laboratory of Urology, the First Affiliated Hospital of Guangzhou Medical University, Guangzhou Medical University, Guangzhou, Guangdong 510230, China*

Jun-Yi Xian − *Department of Urology, Guangzhou Institute of Urology, Guangdong Key Laboratory of Urology, the First Affiliated Hospital of Guangzhou Medical University, Guangzhou Medical University, Guangzhou, Guangdong 510230, China*

Shu-Jue Li − *Department of Urology, Guangzhou Institute of Urology, Guangdong Key Laboratory of Urology, the First Affiliated Hospital of Guangzhou Medical University, Guangzhou Medical University, Guangzhou, Guangdong 510230, China*

Wei-Bo Huang − *Department of Chemistry, Institute of Biomineralization and Lithiasis Research, Jinan University, Guangzhou, Guangdong 510632, China*

Ling-Hong Huang − *Department of Urology, Guangzhou Institute of Urology, Guangdong Key Laboratory of Urology, the First Affiliated Hospital of Guangzhou Medical University, Guangzhou Medical University, Guangzhou, Guangdong 510230, China*

Complete contact information is available at: https://pubs.acs.org/10.1021/acsomega.2c07584

Author Contributions

§B.-X.Y., Y.-H.Z., C.-Y.L. and J.-Y.X. contributed equally to this work.

Notes

The authors declare no competing financial interest.

ACKNOWLEDGMENTS

This work was granted by the Science and Technology Plan Project of Guangzhou (no.: 202102010306 and 202102010165), National Natural Science Foundation of China (no.: 21975105), and Guangdong Provincial Science and Technology Plan Project (no. 2017B030314108).

REFERENCES

(1) Khan, S. R.; Pearle, M. S.; Robertson, W. G.; Gambaro, G.; Canales, B. K.; Doizi, S.; Traxer, O.; Tiselius, H.-G. Kidney stones. *Nat. Rev. Dis. Prim.* **2016**, *2*, 16008.

(2) Tsujihata, M. Mechanism of calcium oxalate renal stone formation and renal tubular cell injury. *Int. J. Urol.* **2008**, *15*, 115−120.

(3) Wesson, J. A.; Ward, M. D. Pathological biomineralization of kidney stones. *Elements* **2007**, *3*, 415−421.

(4) Sun, X.-Y.; Ouyang, J.-M.; Li, Y.-B.; Wen, X.-L. Mechanism of cytotoxicity of micron/nano calcium oxalate monohydrate and dihydrate crystals on renal epithelial cells. *RSC Adv.* **2015**, *5*, 45393−45406.

(5) Qi, S.; Wang, Q.; Xie, B.; Chen, Y.; Zhang, Z.; Xu, Y. P38 MAPK signaling pathway mediates COM crystal-induced crystal adhesion change in rat renal tubular epithelial cells. *Urolithiasis* **2020**, *48*, 9−18.

(6) Lieske, J. C.; Swift, H.; Martin, T.; Patterson, B.; Toback, F. G. Renal epithelial cells rapidly bind and internalize calcium oxalate monohydrate crystals. *Proc. Natl. Acad. Sci. U.S.A.* **1994**, *91*, 6987−6991.

(7) Gombedza, F. C.; Shin, S.; Kanaras, Y. L.; Bandyopadhyay, B. C. Abrogation of store-operated Ca(2+) entry protects against crystal-induced ER stress in human proximal tubular cells. *Cell death discovery* **2019**, *5*, 124.

(8) Hovda, K. E.; Guo, C.; Austin, R.; McMartin, K. E. Renal toxicity of ethylene glycol results from internalization of calcium oxalate crystals by proximal tubule cells. *Toxicol. Lett.* **2010**, *192*, 365−372.

(9) Wu, J.; Tao, Z.; Deng, Y.; Liu, Q.; Liu, Y.; Guan, X.; wang, X. Calcifying nanoparticles induce cytotoxicity mediated by ROS-JNK signaling pathways. *Urolithiasis* **2019**, *47*, 125−135.

(10) Kaleta, B. The role of osteopontin in kidney diseases. *Inflamm. Res.* **2019**, *68*, 93−102.

(11) Kim, D.; Moore, J.; McCoy, C. P.; Irwin, N. J.; Rimer, J. D. Engaging a Battle on Two Fronts: Dual Role of Polyphosphates as Potent Inhibitors of Struvite Nucleation and Crystal Growth. *Chem. Mater.* **2020**, *32*, 8672−8682.

(12) Shirane, Y.; Kagawa, S. Scanning electron microscopic study of the effect of citrate and pyrophosphate on calcium oxalate crystal morphology. *J. Urol.* **1993**, *150*, 1980−1983.

(13) Rimer, J. D.; Kolbach-Mandel, A. M.; Ward, M. D.; Wesson, J. A. The role of macromolecules in the formation of kidney stones. *Urolithiasis* **2017**, *45*, 57−74.

(14) Fischer, V.; Landfester, K.; Muñoz-Espí, R. Stabilization of calcium oxalate metastable phases by oligo (L-glutamic acid): effect of peptide chain length. *Cryst. Growth Des.* **2011**, *11*, 1880−1890.

(15) Akyol, E.; Oner, M. Inhibition of calcium oxalate monohydrate crystal growth using polyelectrolytes. *J. Cryst. Growth* **2007**, *307*, 137−144.

(16) Zhang, D.; Qi, L.; Ma, J.; Cheng, H. Morphological control of calcium oxalate dihydrate by a double-hydrophilic block copolymer. *Chem. Mater.* **2002**, *14*, 2450−2457.

(17) Oner, M.; Calvert, P. The effect of architecture of acrylic polyelectrolytes on inhibition of oxalate crystallization. *Mater. Sci. Eng. C* **1994**, *2*, 93−101.

(18) Moe, O. W. Kidney stones: pathophysiology and medical management. *Lancet* **2006**, *367*, 333−344.

(19) Cai, B.; Wan, P.; Chen, H.; Chen, D.; Chen, X.; Sun, H.; Pan, J. Composition characterization of oyster polysaccharides from Crassostrea hongkongensis and their protective effect against H(2)O(2)-induced oxidative damage in IEC-6 cells. *Int. J. Biol. Macromol.* **2019**, *124*, 246−254.

(20) Wang, L.; Oh, J. Y.; Kim, H. S.; Lee, W.; Cui, Y.; Lee, H. G.; Kim, Y. T.; Ko, J. Y.; Jeon, Y. J. Protective effect of polysaccharides from Celluclast-assisted extract of Hizikia fusiforme against hydrogen

peroxide-induced oxidative stress in vitro in Vero cells and in vivo in zebrafish. *Int. J. Biol. Macromol.* **2018**, *112*, 483−489.
(21) Erturk, E.; Kiernan, M.; Schoen, S. R. Clinical association with urinary glycosaminoglycans and urolithiasis. *Urology* **2002**, *59*, 495−499.
(22) Boevé, E. R.; Cao, L. C.; Verkoelen, C. F.; Romijn, J. C.; de Bruijn, W. C.; Schröder, F. H. Glycosaminoglycans and other sulphated polysaccharides in calculogenesis of urinary stones. *World J. Urol.* **1994**, *12*, 43−48.
(23) Cao, Y. G.; Hao, Y.; Li, Z. H.; Liu, S. T.; Wang, L. X. Antiviral activity of polysaccharide extract from Laminaria japonica against respiratory syncytial virus. *Biomed. Pharmacother.* **2016**, *84*, 1705−1710.
(24) Li, X.; Wang, J.; Zhang, H.; Zhang, Q. Renoprotective effect of low-molecular-weight sulfated polysaccharide from the seaweed Laminaria japonica on glycerol-induced acute kidney injury in rats. *Int. J. Biol. Macromol.* **2017**, *95*, 132−137.
(25) Yan, F.; Hao, H. Effects of Laminaria japonica polysaccharides on exercise endurance and oxidative stress in forced swimming mouse model. *J. Biol. Res.* **2016**, *23*, 7.
(26) Huang, W. B.; Zou, G. J.; Tang, G. H.; Sun, X. Y.; Ouyang, J. M. Regulation of Laminaria Polysaccharides with Different Degrees of Sulfation during the Growth of Calcium Oxalate Crystals and their Protective Effects on Renal Epithelial Cells. *Oxid. Med. Cell. Longev.* **2021**, *2021*, 5555796.
(27) Sun, X. Y.; Ouyang, J. M.; Liu, A. J.; Ding, Y. M.; Gan, Q. Z. Preparation, characterization, and in vitro cytotoxicity of COM and COD crystals with various sizes. *Mater. Sci. Eng., C* **2015**, *57*, 147−156.
(28) Guo, D.; Yu, K.; Sun, X. Y.; Ouyang, J. M. Structural Characterization and Repair Mechanism of Gracilaria lemaneiformis Sulfated Polysaccharides of Different Molecular Weights on Damaged Renal Epithelial Cells. *Oxid. Med. Cell. Longev.* **2018**, *2018*, 7410389.
(29) Zhang, H.; Sun, X. Y.; Chen, X. W.; Ouyang, J. M. Degraded Porphyra yezoensis polysaccharide protects HK-2 cells and reduces nano-COM crystal toxicity, adhesion and endocytosis. *J. Mater. Chem. B* **2020**, *8*, 7233−7252.
(30) Selvaraju, R.; Thiruppathi, G.; Raja, A. FT-IR spectral studies on certain human urinary stones in the patients of rural area. *Spectrochim. Acta Mol. Biomol. Spectrosc.* **2012**, *93*, 260−265.
(31) Huang, S.; Chen, F.; Cheng, H.; Huang, G. Modification and application of polysaccharide from traditional Chinese medicine such as Dendrobium officinale. *Int. J. Biol. Macromol.* **2020**, *157*, 385−393.
(32) Zhao, B.; Tao, F.; Wang, J.; Zhang, J. The sulfated modification and antioxidative activity of polysaccharides from Potentilla anserine L. *New J. Chem.* **2020**, *44*, 4726−4735.
(33) Gunasekaran, S.; Govindan, S.; Ramani, P. Sulfated modification, characterization and bioactivities of an acidic polysaccharide fraction from an edible mushroom Pleurotus eous (Berk.) Sacc. *Heliyon* **2021**, *7*, No. e05964.
(34) Guo, H.; Li, H. Y.; Liu, L.; Wu, C. Y.; Liu, H.; Zhao, L.; Zhang, Q.; Liu, Y. T.; Li, S. Q.; Qin, W.; Wu, D. T. Effects of sulfated modification on the physicochemical properties and biological activities of β-glucans from Qingke (Tibetan hulless barley). *Int. J. Biol. Macromol.* **2019**, *141*, 41−50.
(35) Oliver, J.; MacDowell, M.; Whang, R.; Welt, L. G. The Renal Lesions of Electrolyte Imbalance. *J. Exp. Med.* **1966**, *124*, 263−278.
(36) Khan, S. R.; Hackett, R. L. Calcium oxalate urolithiasis in the rat: is it a model for human stone disease? A review of recent literature. *Scanning Electron. Microsc.* **1985**, *1985*, 24.
(37) Delatte, L.; Miñón-Cifuentes, J.; Medina, J. A. New studies on papillary calculi. *J. Urol.* **1987**, *137*, 1024−1029.
(38) Khan, S. R.; Hackett, R. L. Retention of calcium oxalate crystals in renal tubules. *Scanning Microsc.* **1991**, *5*, 13. discussion 711-2
(39) Yuen, J. W.; Gohel, M. D.; Poon, N. W.; Shum, D. K.; Tam, P. C.; Au, D. W. The initial and subsequent inflammatory events during calcium oxalate lithiasis. *Clin. Chim. Acta* **2010**, *411*, 1018−1026.
(40) Khan, S. R.; Byer, K. J.; Thamilselvan, S.; Hackett, R. L.; McCormack, W. T.; Benson, N. A.; Vaughn, K. L.; Erdos, G. W. Crystal-cell interaction and apoptosis in oxalate-associated injury of renal epithelial cells. *J. Am. Soc. Nephrol.* **1999**, *10*, S457−S463.
(41) Sun, X. Y.; Gan, Q. Z.; Ouyang, J. M. Size-dependent cellular uptake mechanism and cytotoxicity toward calcium oxalate on Vero cells. *Sci. Rep.* **2017**, *7*, 41949.
(42) Zha, X.-Q.; Wang, J.-H.; Yang, X.-F.; Liang, H.; Zhao, L.-L.; Bao, S.-H.; Luo, J.-P.; Xu, Y.-Y.; Zhou, B.-B. Antioxidant properties of polysaccharide fractions with different molecular mass extracted with hot-water from rice bran. *Carbohydr. Polym.* **2009**, *78*, 570−575.
(43) Chen, H.; Zhang, M.; Qu, Z.; Xie, B. Antioxidant activities of different fractions of polysaccharide conjugates from green tea (Camellia Sinensis). *Food Chem.* **2008**, *106*, 559−563.
(44) Wang, D.; Zhang, Y.; Yang, S.; Zhao, D.; Wang, M. A polysaccharide from cultured mycelium of Hericium erinaceus relieves ulcerative colitis by counteracting oxidative stress and improving mitochondrial function. *Int. J. Biol. Macromol.* **2019**, *125*, 572−579.
(45) Zhang, Y. M.; Zhang, L. Y.; Zhou, H.; Li, Y. Y.; Wei, K. X.; Li, C. H.; Zhou, T.; Wang, J. F.; Wei, W. J.; Hua, J. R.; He, Y.; Hong, T.; Liu, Y. Q. Astragalus polysaccharide inhibits radiation-induced bystander effects by regulating apoptosis in Bone Mesenchymal Stem Cells (BMSCs). *Cell cycle* **2020**, *19*, 3195−3207.
(46) Yu, F.; Chen, Z.; Wang, B.; Jin, Z.; Hou, Y.; Ma, S.; Liu, X. The role of lysosome in cell death regulation. *Tumour Biol.* **2016**, *37*, 1427−1436.
(47) Kunishige, R.; Mizoguchi, M.; Tsubouchi, A.; Hanaoka, K.; Miura, Y.; Kurosu, H.; Urano, Y.; Kuro-o, O. M.; Murata, M. Calciprotein particle-induced cytotoxicity via lysosomal dysfunction and altered cholesterol distribution in renal epithelial HK-2 cells. *Sci. Rep.* **2020**, *10*, 20125.
(48) Hou, K.; Yu, Q.; Hu, X.; Ding, X.; Hong, J.; Chen, Y.; Xie, J.; Nie, S.; Xie, M. Protective effect of Ganoderma atrum polysaccharide on acrolein-induced macrophage injury via autophagy-dependent apoptosis pathway. *Food Chem. Toxicol.* **2019**, *133*, 110757.

https://doi.org/10.1021/acsomega.2c07584
ACS Omega 2023, 8, 7816−7828